Running title: **Light regulation of β-carboxysome biosynthesis**

Correspondence: **Lu-Ning Liu**

Institute of Integrative Biology
University of Liverpool
United Kingdom

Address: Bioscience Building, Crown Street, Liverpool L69 7ZB, United Kingdom
Tel: +44 (0)151 795 4426
E-mail: luning.liu@liverpool.ac.uk

Research area: Membranes, Transport and Biogenetics

Light modulates the biosynthesis and organization of cyanobacterial carbon fixation machinery through photosynthetic electron flow[1]

Yaqi Sun, Selene Casella, Yi Fang, Fang Huang, Matthew Faulkner, Steve Barrett, and Lu-Ning Liu

Institute of Integrative Biology, University of Liverpool, Liverpool L69 7ZB, United Kingdom (Y.S., S.C., Y.F., F.H., M.F., L.-N.L.), Department of Physics, University of Liverpool, Liverpool L69 7ZE, United Kingdom (S.B.)

One-sentence summary:

The biosynthesis and spatial positioning of β-carboxysomes, the carbon fixation machinery in cyanobacteria, are modulated by light intensity and redox state of photosynthetic electron transport chain.

Footnotes:

[1] Y.S. acknowledges a University of Liverpool−China Scholarship Council scholarship. L.-N.L. acknowledges a Royal Society University Research Fellowship (UF120411), a Royal Society Research grant for URF (RG130442), a Royal Society International Exchanges grant (IE131399) and a Biotechnology and Biological Sciences Research Council grant (BB/M024202/1).

*** Corresponding author**:

Lu-Ning Liu, E-mail: luning.liu@liverpool.ac.uk

Keywords:

Bacterial microcompartment; Biosynthesis; Carbon fixation; Carboxysome; Cyanobacteria; Light regulation; Photosynthetic electron transport; Redox regulation; RuBisCO; Spatial positioning

ABSTRACT

Cyanobacteria have evolved effective adaptive mechanisms to improve photosynthesis and CO_2 fixation. The central CO_2-fixing machinery is the carboxysome, which is composed of an icosahedral proteinaceous shell encapsulating the key carbon fixation enzyme, ribulose-1,5-bisphosphate carboxylase/oxygenase (RuBisCO), in the interior. Controlled biosynthesis and ordered organization of carboxysomes are vital to the CO_2-fixing activity of cyanobacterial cells. However, little is known about how carboxysome biosynthesis and spatial positioning are physiologically regulated to adjust to dynamic changes in the environment. Here, we used fluorescence tagging and live-cell confocal fluorescence imaging to explore the biosynthesis and subcellular localization of β-carboxysomes within a model cyanobacterium, *Synechococcus elongatus* PCC7942, in response to light variation. We demonstrated that β-carboxysome biosynthesis is accelerated in response to increasing light intensity, thereby enhancing the carbon fixation activity of the cell. Inhibition of photosynthetic electron flow impairs the accumulation of carboxysomes, indicating a close coordination between β-carboxysome biogenesis and photosynthetic electron transport. Likewise, the spatial organization of carboxysomes in the cell correlates with the redox state of photosynthetic electron transport chain. This study provides essential knowledge for us to modulate the β-carboxysome biosynthesis and function in cyanobacteria. In translational terms, the knowledge is instrumental for design and synthetic engineering of functional carboxysomes into higher plants to improve photosynthesis performance and CO_2 fixation.

INTRODUCTION

Compartmentalization of metabolic pathways in cells provides the fundamental basis for enhancing and modulating the cellular metabolism. Many prokaryotes have evolved specialized metabolic organelles, known as bacterial microcompartments, to sequester key metabolic pathways and thereby improve the efficiency of metabolic activities (for reviews see Kerfeld et al., 2010; Bobik et al., 2015). Unlike eukaryotic organelles, bacterial microcompartments are assembled entirely by proteins. These organelles consist of interior enzymes that catalyze sequential metabolic reactions (Yeates et al., 2010), surrounded by a single-layer proteinaceous shell (Kerfeld et al., 2005; Tsai et al., 2007; Tanaka et al., 2008; Sutter et al., 2015). The shell facets are composed of hexameric and pentameric proteins, resulting in an overall shell architecture resembling an icosahedral viral capsid (Kinney et al., 2011; Hantke et al., 2014; Kerfeld and Erbilgin, 2015). Interactions between shell proteins are important for the self-assembly of the shell (Sutter et al., 2015). The selectively permeable shell serves to concentrate enzymes and substrates, mediate flux of metabolites, modulate the redox state, and prevent toxic intermediates from diffusing into the cytoplasm (Havemann et al., 2002; Yeates et al., 2008).

Carboxysomes were the first bacterial microcompartments to be discovered, and are widely distributed among cyanobacteria and some chemoautotrophs as the central machinery for the fixation of carbon dioxide (Shively et al., 1973). Two different types of carboxysomes have been identified (α- and β-carboxysomes), according to the types of the CO_2-fixing enzyme, ribulose-1,5-bisphosphate carboxylase/oxygenase (RuBisCO, form 1A and form 1B), possessed in cyanobacteria. In most β-cyanobacteria, RuBisCO is sequestered in the β-carboxysome lumen by a shell that is composed of shell and shell-associated proteins encoded by a *ccmKLMNO* operon (Omata et al., 2001; Long et al., 2010; Rae et al., 2012). The carboxysomal carbonic anhydrase is colocalized with RuBisCO in the β-carboxysome, serving to create a CO_2-rich microenvironment to favor the RuBisCO activity. Some cyanobacterial species do not have the carboxysomal β-carbonic anhydrase (CcaA) homologs; instead the N-terminal domain of CcmM functions as an active γ-

carbonic anhydrase (Peña et al., 2010). The shell facets act as a selective barrier that allows the diffusion of HCO_3^- and retains CO_2 in the interior (Dou et al., 2008). Through these mechanisms, carboxysomes elevate the CO_2 concentration in the vicinity of RuBisCO, and thereby enhance the efficiency of carbon fixation. Supported by this nano-scale CO_2-fixing machinery, cyanobacteria contribute more than 25% of global carbon fixation (Field et al., 1998; Liu et al., 1999).

The efficiency of carboxysomes in enhancing carbon fixation has attracted tremendous interest to engineering the CO_2-fixing organelle in other organisms. For example, introducing β-carboxysomes into higher plants that use the ancestral C_3 pathway of photosynthesis could potentially enhance photosynthetic carbon fixation and crop production (Lin et al., 2014a; Lin et al., 2014b). However, engineering of functional carboxysomes requires extensive understanding about the principles underlying the formation of β-carboxysomes and the physiological integration of β-carboxysomes into the cellular metabolism.

Indeed, cyanobacterial cells have evolved comprehensive systems to regulate the biosynthesis and spatial organization of carboxysomes, allowing them to modulate the capacity for photosynthetic carbon fixation. Recent studies elucidated that the β-carboxysome assembly is initiated from the packing of RuBisCO enzymes, followed by the encapsulation of peripheral shell proteins (Cameron et al., 2013; Chen et al., 2013). In the model rod-shaped cyanobacterium, *Synechococcus elongatus* PCC7942 (hereafter *Synechococcus*), three to four β-carboxysomes were observed to be evenly spaced along the centerline of the longitudinal axis of cells, ensuring the equal segregation of the machinery between daughter cells (Savage et al., 2010). Such specific organization of carboxysomes within cyanobacterial cells is likely to be determined by the interaction between carboxysomes and the cytoskeleton (Savage et al., 2010). Advanced understanding of the functions and assembly of β-carboxysome proteins has recently led to the construction of a chimeric protein that can functionally replace four native proteins (CcmM58, CcmM35, CcaA and CcmN) required for carboxysome formation (Gonzalez-Esquer et al., 2015). These findings outlined the self-assembly nature and integration of carboxysomes in the cell.

However, how β-carboxysome biosynthesis and organization are physiologically regulated in cyanobacteria in response to environmental changes remains poorly understood.

Here, using a combination of live-cell confocal fluorescence microscopy, biochemical and physiological approaches, we investigated the formation and spatial positioning of β-carboxysomes in *Synechococcus* under varying light intensities. Our study provides new insights into the regulation of β-carboxysome biosynthesis by light and the roles of photosynthetic electron flow in the carboxysome assembly. Knowledge obtained from this work is fundamental to the bioengineering and modulation of functional carboxysomes to boost photosynthetic carbon fixation in dynamic and diverse environments.

RESULTS

We chose *Synechococcus* as the model organism due to its superior genetic tractability and proven suitability for fluorescence imaging (Savage et al., 2010; Liu et al., 2012; Cameron et al., 2013; Cohen et al., 2014). RbcL, the large subunit of RuBisCO that resides in the β-carboxysome lumen, was tagged at the C-terminus with enhanced green fluorescent protein (eGFP), and was visualized under confocal fluorescence microscopy to characterize the formation and positioning of carboxysomes *in vivo*. Homologous recombination was utilized to tag the genes at their native chromosomal locus under the control of their native promoters (Supplemental Fig. S1). This ensures that the fluorescently tagged proteins were expressed in context and at physiological levels.

Fig. 1 represents the confocal images of RbcL:eGFP *Synechococcus* strain. The eGFP fluorescence (green) indicates the subcellular localization of carboxysomes, and the endogenous chlorophyll fluorescence (red) shows the organization of thylakoid membranes. In addition, the specific DNA-staining dye, 4',6-diamidino-2-phenylindole (DAPI), was used to image chromosomes, offering the possibility to determine the cytoplasmic environment in cyanobacteria (Fig. 1A). The merged channel shows that most of the cytoplasmic volume of the *Synechococcus* cell is densely occupied by carboxysomes and chromosomes, and no significant fluorescence gaps were visible, implying that all carboxysomes in the RbcL:eGFP transformant are likely fluorescently visible using confocal microscopy. In the free-eGFP expressing *Synechococcus* construct, the eGFP fluorescence is evenly spread across the cytoplasm. The distinct distributions of GFP fluorescence in the RbcL:eGFP and free-eGFP expressing *Synechococcus* strains indicate the self-assembly of carboxysome proteins. PCR and immunoblot results indicate the RbcL:eGFP transformant could not be fully segregated; about 30% of total RbcL were fused with eGFP (Supplemental Fig. S1). The addition of GFP tag might limit the number of RuBisCO proteins accommodated within the carboxysomal interior (Menon et al., 2010). Thus, there seems to be a regulation to avert full segregation and retain some unlabeled RuBisCO in the carboxysome. Nevertheless, the fluorescence tagging did not affect the growth of cyanobacterial cells

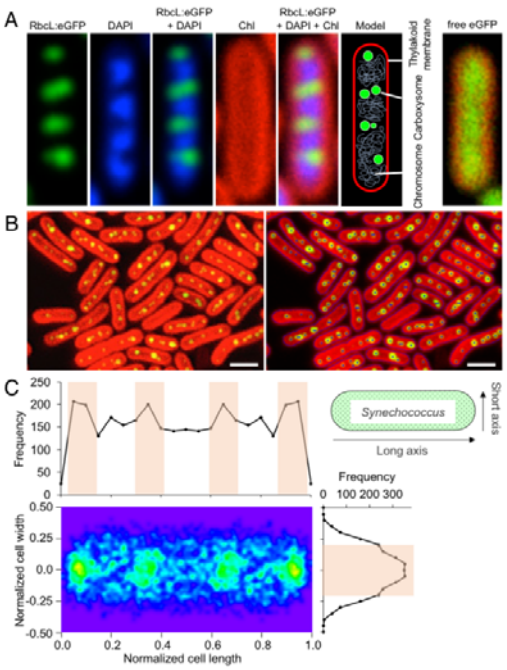

Figure 1. Spatial organization of β-carboxysomes in RbcL:eGFP *Synechococcus* cells. A, Confocal images of a RbcL:eGFP *Synechococcus* cell. Green, eGFP labelled carboxysomes; blue, 4',6-diamidino-2-phenylindole (DAPI) stained DNA; red, auto-fluorescence of the thylakoid membrane. The merged channel revealed that most of the cytoplasmic volume of the *Synechococcus* cell is occupied by carboxysomes and chromosomes. This subcellular organization indicated that all carboxysomes in the RbcL:eGFP cell can been visualized using confocal microscopy. The confocal image of the *Synechococcus* construct that expresses free eGFP illustrates that free eGFP are spread throughout the cytoplasm without specific aggregation. B, Computational programming of image analysis allows automatic identification of carboxysomes in cells in confocal images. Scale bar: 2 μm. C, Statistical determination of the spatial localization of carboxysomes within the cell revealed the distribution profiles of carboxysomes along both the longitudinal and short axes of the cell (n = 300). The orange squares represent the relative frequency of carboxysome localization in the cell. The developed automated analysis software routines were used in this work for analyzing the carboxysome content and positioning.

(Supplemental Fig. S1). Analysis of confocal images was programmed to examine statistically the number and spatial positioning of carboxysomes in the cell (Fig. 1B and Fig. 1C, n = 300). On average, there are about four evenly positioned carboxysomes per cell, consistent with previous observation (Savage et al., 2010), confirming the physiological state of RbcL:eGFP cells. We also labeled the minor shell proteins in the carboxysome, CcmK4 (Kerfeld et al., 2005; Savage et al., 2010; Cai et al., 2015), using eGFP. PCR results demonstrate that the *ccmK4:egfp* transformant was fully segregated, and the construct has similar growth rates compared to wild-type and RbcL:eGFP strains (Supplemental Fig. S1).

To examine whether the GFP-labelled carboxysomes can be physiologically regulated within cells, we assayed the impact of CO_2 concentration on the formation of carboxysomes. Previous studies have indicated that the carboxysomes content is affected by CO_2 availability (McKay et al.,

1993; Harano et al., 2003; Woodger et al., 2003; Whitehead et al., 2014). Our confocal images show a striking reduction in the numbers of carboxysomes in cells aerated with 3% CO_2, compared to those in cells grown in ambient air (Supplemental Fig. S2). It reveals the feasibility of using live-cell confocal imaging to monitor the *in vivo* regulation of carboxysome biosynthesis in response to environmental change.

Light triggers carboxysome biosynthesis

We studied the spatial distribution of carboxysomes in *Synechococcus* under the variation of light intensity, low light (LL, 10 $\mu E \cdot m^{-2} \cdot s^{-1}$), moderate light (ML, 50 $\mu E \cdot m^{-2} \cdot s^{-1}$) and higher light (HL, 100 $\mu E \cdot m^{-2} \cdot s^{-1}$). Confocal images of RbcL:eGFP cells show that the carboxysome abundance per cell has a strong correlation with the illumination intensity during cell growth (Fig. 2A). The number of carboxysomes per cell is higher under HL, whereas LL leads to the reduction in carboxysome numbers. The light-dependence of carboxysome content was further substantiated by transmission electron microscopy results of wild-type *Synechococcus* cells (Fig. 2B, Supplemental Fig. 3). The numbers and positioning of carboxysomes in the cell were statistically analyzed based on the confocal images. On average, around two carboxysomes per cell (1.8 ± 1.2, n = 500) were observed under LL, whereas about four carboxysomes per cell (4.4 ± 1.9, n = 500) under ML and over ten (10.4 ± 3.8, n = 500) under HL were detected (Fig. 2C). The data is in good agreement with the results from electron microscopy images (Supplemental Fig. 3): 1.6 ± 0.7 (LL, n = 30), 3.9 ± 0.8 (ML, n = 30), 10.2 ± 2.0 (HL, n = 30). No significant changes in cell dimensions were detected under different light intensities (Supplemental Fig. S4). These results indicate that light intensity plays an important role in determining the biosynthesis of β-carboxysomes in *Synechococcus*.

Varying light intensities could also result in different organizational patterns of carboxysomes in cells. Image analysis reveals even distribution of carboxysomes along the longitudinal axis of the cell (Fig. 2D). Carboxysomes tend to locate at approximately one forth position along the cell

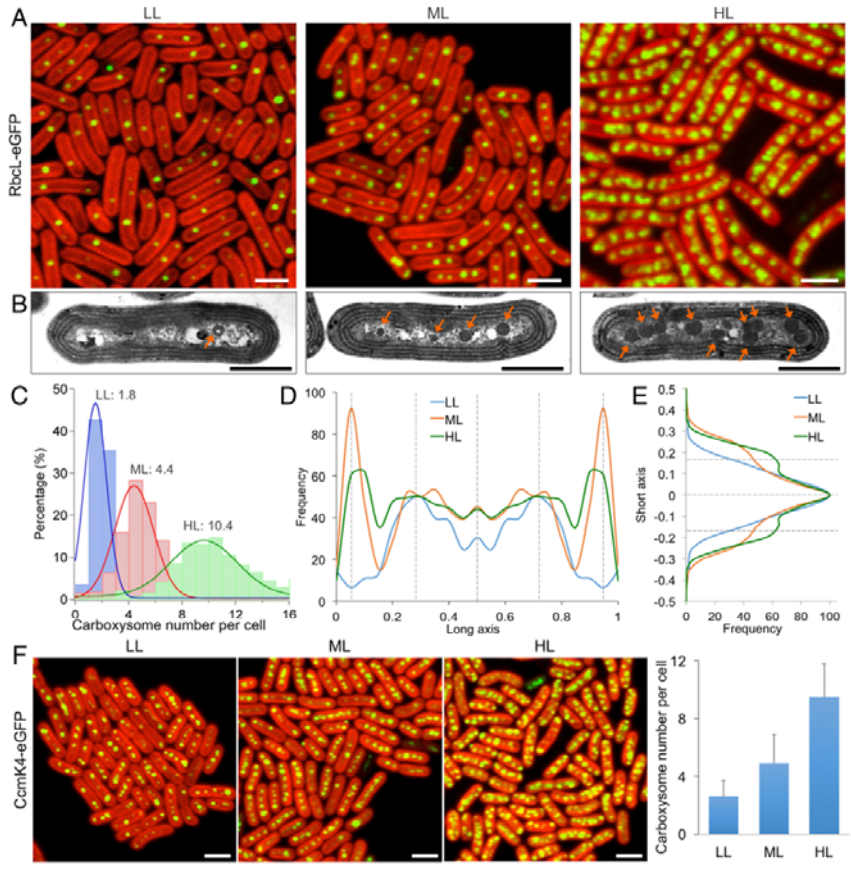

Figure 2. Distinct distribution patterns of carboxysomes in *Synechococcus* under different light intensities. A, Confocal microscopy images of the spatial organizations of carboxysomes in the RbcL:eGFP strain grown under low light (LL, 10 μE·m^{-2}·s^{-1}), moderate light (ML, 50 μE·m^{-2}·s^{-1}) and higher light (HL, 100 μE·m^{-2}·s^{-1}). Variations in the carboxysome content were observed under different light intensities. Scale bar: 2 μm. B, Thin-section transmission electron microscopy images of wild-type *Synechococcus* cells grown under LL, ML and HL (see Supplemental Fig. 3). The thylakoid membranes form regular multiple parallel layers surrounding the cytoplasm. The carboxysomes were observed as dark polyhedral particles (arrows) in the cytoplasm. Stronger light leads to the increase in carboxysome numbers in cells. Scale bar: 1 μm. C, Computational analysis of confocal images shows the average numbers of carboxysomes per cell under LL, ML and HL (n = 500 for each condition). D, The positioning of carboxysomes along the normalized longitudinal axis of the *Synechococcus* cell under LL, ML and HL. The relatively periodic and polar localization of carboxysomes in cells were indicated (n = 500). E, The positioning of carboxysomes along the normalized short axis of the *Synechococcus* cell (n = 500). HL gives rise to a wider distribution of carboxysomes from the centerline of cells. F, Confocal microscopy images of CcmK4:eGFP cells show the spatial positioning of carboxysomes grown under LL, ML and HL. Variations in the carboxysome content were observed under different light intensities, in good agreement with those of the RbcL:eGFP strain. Error bars represent standard deviation (SD, n = 500 for each condition). Scale bar: 2 μm.

length under LL, whereas under ML and HL a polar location of carboxysomes within the cell was observed apart from the even distribution (Fig. 2D). Analysis of the positioning of carboxysomes along the cell width elucidates that increasing numbers of carboxysomes induced by stronger light present a wider distribution along the short axis of the cell, compared to the centerline positioning observed under LL (Fig. 2E). This organization likely provides a means to house more carboxysomes in a spatially crowded cytoplasm environment. Consistent with the results of the RbcL:eGFP construct, our confocal images of the CcmK4:eGFP construct also show the increase in carboxysome content triggered by stronger irradiance (Fig. 2F, n = 500). Similarly, light regulation

of carboxysome content in *Synechococcus* was also seen in the RbcL:YFP strain (Savage et al., 2010) in which *rbcL:yfp* was inserted into a neutral site rather than the native locus in the genome (Supplemental Fig. 5). Together, our observations reveal a general regulation of carboxysome content and organization in *Synechococcus* in response to variations in light intensity.

The light-regulated carboxysome biosynthesis was further characterized by time-lapse confocal imaging during cell growth (Fig. 3). HL treatment on cells that were pre-adapted to LL resulted in a linear increase in carboxysome content over five days. Reversibly, LL treatment caused a reduction in carboxysome numbers, although the rate of reduction is lower than that of the increase in carboxysome numbers. These results indicate that the light-dependent carboxysome biogenesis might function as a long-term acclimation process in cyanobacteria. On the other hand, despite potential repairing mechanism led by protein dynamics (Sutter et al., 2015), there appears to be no specific degradation pathway for carboxysomes. The stability of mature carboxysomes *in vivo* may be of physiological importance for the cellular metabolism (Cameron et al., 2013).

Light-induced carboxysome biosynthesis determines the carbon fixation activity of cells

In addition to the confocal microscopy results that reveal the light-induced carboxysome content in the cell, immunoblot analysis show that the abundance of RuBisCO proteins per cell, normalized using the AtpB content (Zhang et al., 2012), is also up-regulated by increasing irradiance (Fig. 4A). The RuBisCO abundance under HL is about six and two times as high as those under LL and ML, respectively (Fig. 4B and Fig. 4C, $n = 6$). Interestingly, slight increase in RuBisCO content was observed in both RbcL:eGFP and CcmK4:eGFP strains compared to WT cells, probably as compensation for compromised CO_2-fixing activities of carboxysomes caused by fluorescence labelling. The light-induced changes in RuBisCO content at the protein level was also confirmed by measuring the total fluorescence intensity of RbcL:eGFP per cell (Supplemental Fig. S6). Our results corroborate previous studies, which revealed that the transcription of carboxysome genes is stimulated in response to increasing light intensity (Watson and Tabita, 1996; Hihara et al.,

2001; Gill et al., 2002; Huang et al., 2002; McGinn et al., 2004).

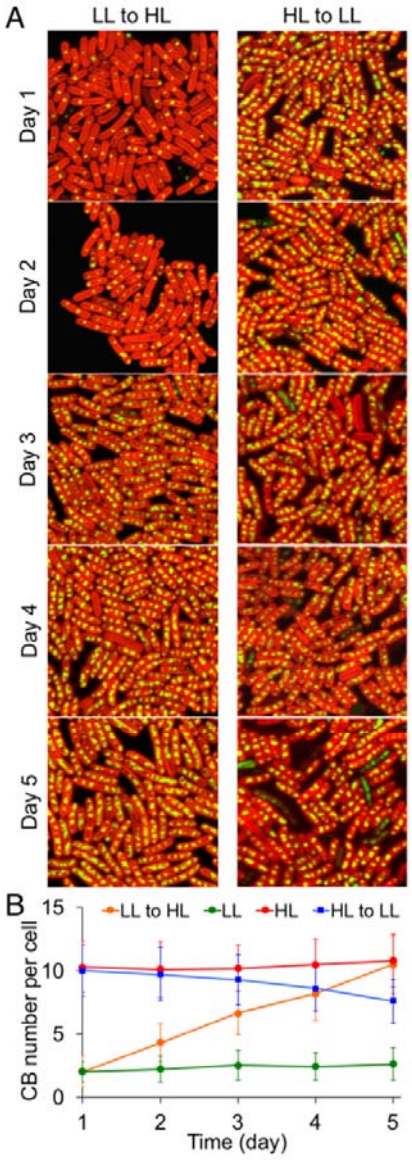

Figure 3. Characterization of the light-regulated biosynthesis process of β-carboxysomes. A, Time-lapse confocal images of the LL-adapted RbcL:eGFP *Synechococcus* strain under HL treatment and the HL-adapted RbcL:eGFP strain under LL treatment. Cells from the same flasks were imaged under confocal microscopy once per day, for continuously 5 days. Changes in carboxysome content per cell were captured. B, Analysis of the average numbers of carboxysomes based on confocal images reveals an increase in carboxysome abundance induced by HL and a decline in carboxysome abundance caused by LL, compared to the numbers of carboxysomes under constant LL or HL treatments. Error bars represent SD (n = 250).

To verify the physiological coordination between carboxysome content and carbon fixation in *Synechococcus*, we surveyed the carbon fixation activities of cells (based on the AtpB content) under different light conditions. 0.5 mM D-ribulose 1,5-bisphosphate sodium salt hydrate (RuBP) was applied to examine the maximum carbon fixation rates (Supplemental Fig. S7). Fig. 4C depicts

a strong dependence of carbon fixation rates of *Synechococcus* cells on light intensity. The carbon

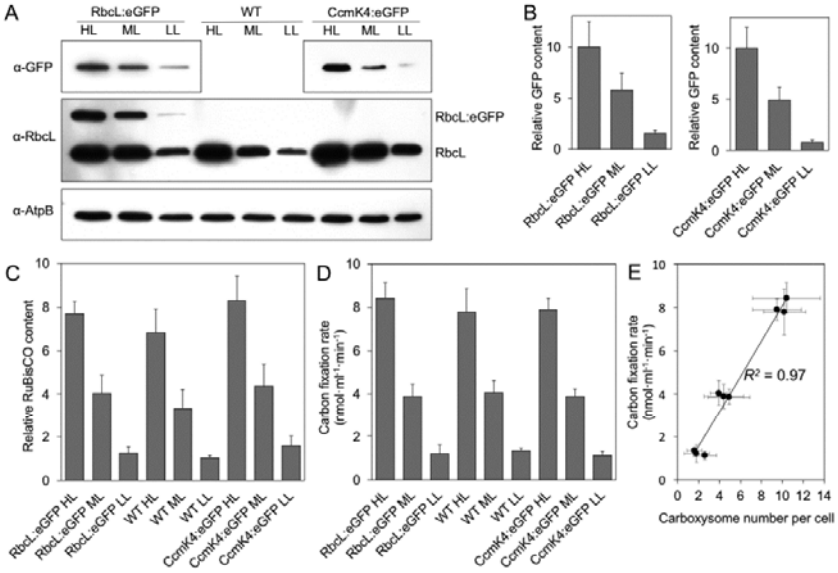

Figure 4. Light modulates the biosynthesis of β-carboxysomes and cellular carbon fixation in *Synechococcus*. A, Immunoblot analysis using anti-RbcL and anti-GFP antibodies shows variations of the RuBisCO content in RbcL:eGFP cells. HL triggers the accumulation of RuBisCO. Using anti-RbcL antibody RbcL:eGFP strains present two bands: the upper band for RbcL-eGFP and the lower band for RbcL only. AtpB was used as a loading control (Zhang et al., 2012). Gels are representative of six independent experiments. B, Immunoblot analysis implies that the GFP amount in RbcL:eGFP and CcmK4:eGFP cells varies under different light intensities (± SD, $n = 6$, $P < 0.05$). C, Densitometry of RbcL in wild-type, RbcL:eGFP and CcmK4:eGFP cells is dependent on light intensity (± SD, $n = 6$, $P < 0.05$). D, ^{14}C carbon fixation rates of wild-type, RbcL:eGFP and CcmK4:eGFP cells under LL, ML and HL at 0.5 mM D-ribulose 1,5-bisphosphate sodium salt hydrate (RuBP, ± SD, $n = 6$). The cell density was normalized using the AtpB content (Fig. 4A). The carbon fixation rates of cells as a function of RuBP is shown in Supplemental Fig. S7. E, The carbon fixation rate per cell is proportional to the numbers of carboxysomes within the cell ($R^2 = 0.97$). The numbers of carboxysomes per cell were determined from electron microscopy images for the wild-type strain, and confocal microscopy images for RbcL:eGFP and CcmK4:eGFP strains.

fixation rate of wild-type cells in HL (7.8 μmol·min^{-1}·ml^{-1}) is higher compared with those in ML (4.0 μmol·min^{-1}·ml^{-1}) and LL (1.3 μmol·min^{-1}·ml^{-1}) ($n = 6$, Fig. 4D). Similar tendency was also observed in RbcL:eGFP and CcmK4:eGFP cells, indicating that increasing irradiance enhances the carbon fixation of *Synechococcus* cells ($n = 6$, Fig. 4D). Furthermore, there is a close correlation between the numbers of carboxysomes and carbon fixation rate of cells (Fig. 4E). Together, our results indicate explicitly that the light-intensity-regulated carboxysome biosynthesis serves as a regulatory mechanism of modulating the capacity of CO_2 fixation in the cell.

Light regulation of carboxysome biosynthesis is mediated by photosynthetic electron flow

Changes in light intensity could alter electron flow and redox states of intersystem electron carriers, especially the plastoquinone (PQ) pool (Mullineaux, 2001; Liu et al., 2012). We conducted extensive studies on the carboxysome formation process in response to irradiance variations in the presence of two specific inhibitors of photosynthetic electron transport, namely 3-(3,4-

dichlorophenyl)-1,1-dimethylurea (DCMU) and 2,5-dibromo-3-methyl-6-isopropyl-benzoquinone

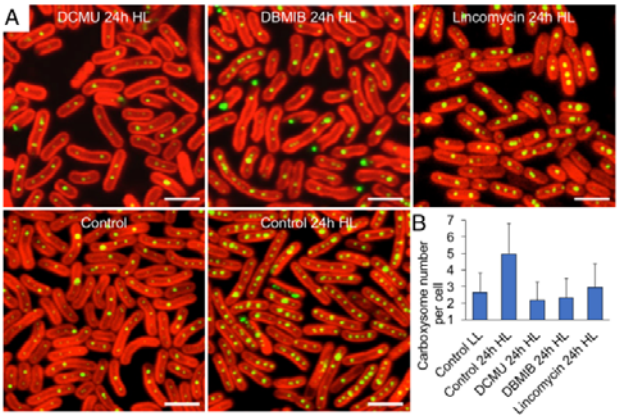

Figure 5. β-carboxysome biosynthesis is regulated by photosynthetic electron flow. A, Confocal microscopy images of LL-adapted RbcL:eGFP *Synechococcus* cells after 24-hour HL treatment, in the presence of the photosynthetic electron transport inhibitors DCMU, DBMIB or the protein synthesis inhibitor lincomycin. The control images were captured in LL-adapted *Synechococcus* cells grown at LL and after 24-hour HL treatment without inhibitor treatments. Scale bar: 2 μm. B, Analysis of the average numbers of carboxysomes per cell (± SD, n = 300) based on the confocal images illustrates the suppression of carboxysome content with the treatments of DCMU and DBMIB, indicating that light intensity regulates the biosynthesis and assembly of carboxysomes through photosynthetic electron flux.

(DBMIB). DCMU and DBMIB inhibit photosynthetic electron transport from the photosystem II complex to the PQ pool and from the PQ pool to the cytochrome b_6f complex, respectively (Trebst, 1980). We observed that when light is switched from LL to HL for 24 hours, both DCMU and DBMIB treatments suppress the O_2 evolution from photosystem II of cells (Supplemental Fig. 8), and hampers the light-induced carboxysome biosynthesis (Fig. 5). It demonstrates that the inhibition of photosynthetic electron flow impairs the biogenesis of carboxysomes in cyanobacteria. The increase in carboxysome content in the cell was also inhibited by lincomycin (Fig. 5), a protein synthesis inhibitor that suppresses *de novo* protein synthesis (Dalla Chiesa et al., 1997). The similar effects of DCMU, DBMIB and lincomycin on impeding the carboxysome biosynthesis suggest that the regulation of photosynthetic electron flow may affect the synthesis and assembly of carboxysome proteins to form carboxysomes.

Carboxysome localization is sensitive to the redox state of photosynthetic electron transport

Closer inspection of the distribution of carboxysomes in HL-adapted cells illustrates that along with the dense packing of carboxysomes in the cytoplasm, a few carboxysomes aggregate preferentially and form a single large carboxysome "cluster". Several "clusters" are then evenly

positioned along the longitudinal axis of the cell (Fig. 6A). It was postulated that the local CO_2

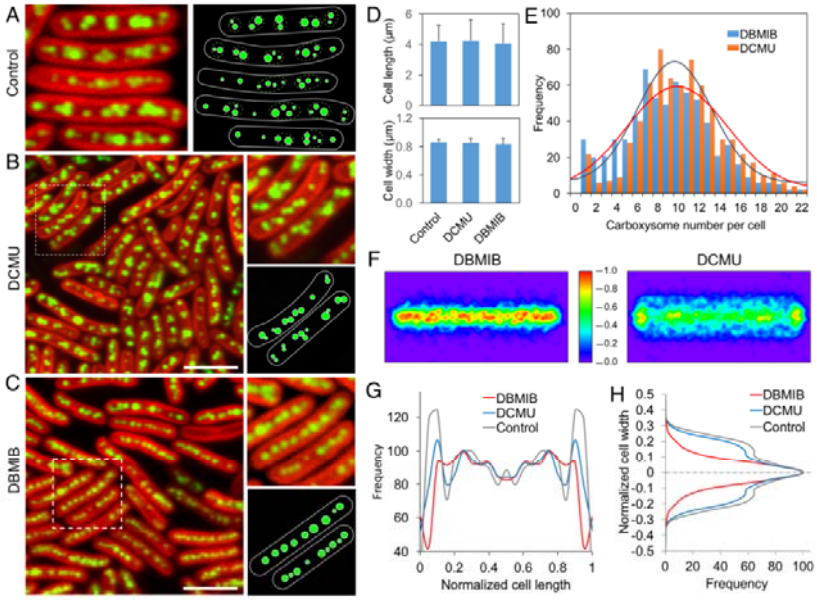

Figure 6. Correlation between the spatial organization of β-carboxysomes and redox state of photosynthetic electron transport chain in *Synechococcus*. A, Confocal image (left) and schematic model (right) of the HL-adapted RbcL:eGFP strain show the evenly distributed carboxysome "clusters" (orange dotted circles), each of which contains several carboxysomes assembled together in the local cytoplasmic region. B, Confocal image of HL-adapted RbcL:eGFP cells under DCMU treatment shows the clustering distribution of carboxysomes along the centerline of the cell. Scale bar: 5 μm. C, Confocal image of HL-adapted *Synechococcus* cells under DBMIB treatment shows the linear distribution of carboxysomes along the centerline of the cell. Scale bar: 5 μm. D, No significant changes in the cell length and width of *Synechococcus* is detected during inhibitor treatments for 24 hours ($P > 0.05$, $n = 500$). Error bars represent SD. E, Average numbers of carboxysomes per cell under the treatments of DCMU and DBMIB do not have remarkable changes ($P > 0.05$, $n = 500$). F, Normalized spatial distribution maps of carboxysomes in cells under the treatments of DCMU and DBMIB. The scale bar presents the relative frequency of carboxysome localization. G, The distributions of carboxysomes along the cell length under DCMU and DBMIB treatments ($n = 500$). H, DBMIB treatment results in a linear positioning of carboxysomes at the centerline of HL-adapted *Synechococcus* cells, whereas the DCMU treatment leads to a wider distribution of carboxysomes along the cell width ($n = 500$). Similar results were also obtained in LL- and ML-adapted *Synechococcus* cells (Supplemental Fig. S9) and CcmK4:eGFP cells (Supplemental Fig. 10).

concentration near each carboxysome is higher (Mangan and Brenner, 2014). The carboxysome clusters may be functionally advantageous to minimizing CO_2 leakage and maximizing the CO_2 accumulation around all carboxysomes in the cytoplasm (Ting et al., 2007), thereby enhancing carbon fixation of cells. The equally spaced carboxysome "clusters" along the long axis of the cell may correlate with the positioning of chromosomes (Jain et al., 2012). It could favor the equal segregation of carboxysomes between daughter cells during cell division (Savage et al., 2010).

We further surveyed the effects of DCMU and DBMIB on the spatial organization of carboxysomes in cells. In HL-adapted RbcL:eGFP cells, carboxysomes possess a dense distribution, suitable for detecting the spatial redistribution of carboxysomes. Under DCMU treatment, carboxysomes present the typical "clustering" distribution in the cytoplasm (Fig. 6B), similar to the observations in non-treated cells. By contrast, DBMIB treatment gave rise to a linear positioning of carboxysomes along the centerline of the cell (Fig. 6C). Image analysis reveals that, relative to the

marked re-positioning of carboxysomes, no detectable differences in the thylakoid membrane structure and cytoplasmic volume (indicated by endogenous chlorophyll fluorescence) were observed (Fig. 6D), whereas the carboxysome numbers per cell under DCMU and DBMIB treatments were comparable (Fig. 6E). The periodic distribution of carboxysomes along the long axis of DBMIB-treated cells is somewhat less significant than that of DCMU-treated cells, and the polar localization of carboxysomes seems to disappear in DBMIB-treated cells (Fig. 6F and Fig. 6G). More remarkable changes were observed in carboxysome distribution along the short axis of the cell (Fig. 6F and Fig. 6H). DBMIB treatment led to the relocation of carboxysomes from a wider distribution along the cell width to a narrow positioning at the centerline of the short axis of the cell, compared to the wide distribution observed in DCMU-treated and non-treated cells (Fig. 6H). DCMU and DBMIB have opposite effects on the redox state of PQ pool in photosynthetic electron transport chain: the PQ pool is oxidized by DCMU and reduced by DBMIB. The distinct effects of DCMU and DBMIB indicate that the spatial organization of β-carboxysomes in *Synechococcus* correlates with the redox state of photosynthetic electron transport chain. Consistent with the finding of HL-adapted cells, the reorganization of carboxysomes under DCMU and DBMIB treatments was also observed in LL- and ML-adapted RbcL:eGFP cells (Supplemental Fig. S9) and CcmK4:eGFP cells (Supplemental Fig. 10), corroborating that the redox regulation of photosynthetic electron flow could affect the spatial positioning of β-carboxysomes in *Synechococcus*. We further observed that changes in carboxysome localization are not clearly visible within 4-hour DBMIB treatment (Supplemental Fig. 11), implying that the reorganization of carboxysomes seems to be a long-term adaptive process in response to redox regulation.

DISCUSSION

In cyanobacteria, light is fundamental to energy production, DNA replication and the regulation of gene expression (Asayama, 2006; Ohbayashi et al., 2013). Light-dependent reactions of photosynthesis generate chemical energy, in the forms of ATP and NADPH, which is utilized to drive the Calvin-Benson-Bassham Cycle responsible for CO_2 fixation into metabolizable sugars. It was found that HL could induce an increase in the transcription of RuBisCO and carboxysome *ccm* genes (Watson and Tabita, 1996; Hihara et al., 2001; Gill et al., 2002; Huang et al., 2002). In the present work, we evaluated the impact of light intensity on the regulation of β-carboxysome biosynthesis at the whole organelle and cellular levels. Our results show that increasing irradiance triggers the expression of carboxysome proteins (Fig. 4A, Supplementary Fig. S6) and formation of functional carboxysomes (Fig. 2), thereby enhancing carbon fixation of cells (Fig. 4). We further revealed the close correlation between light-regulated photosynthetic electron flow and β-carboxysome biosynthesis (Fig. 5). Given that the expression of carboxysome genes and their encoded proteins are under light-dark regulation (Watson and Tabita, 1996; Ito et al., 2009; Aryal et al., 2011), further work needs to be directed to elucidate whether *de novo* assembly of carboxysomes is regulated and/or potentially gated by the cyanobacterial circadian rhythm.

The spatial distribution of β-carboxysomes along the longitudinal axis of *Synechococcus* cells is driven by interactions with the cytoskeleton, ensuring the equal segregation of carbon fixation organelles between daughter cells (Savage et al., 2010). *Synechococcus* cytoplasm densely accommodates carboxysomes and chromosomes, which are interspersed with each other (Fig. 1A). It is conceivable that the organization and dynamics of carboxysomes correlate with the partitioning of chromosomes. On the other hand, the disruption of *parA* resulted in unequal positioning of carboxysomes, but did not interfere with chromosome organization, suggesting that the spatial partitioning of carboxysomes and chromosomes in *Synechococcus* is likely regulated separately (Jain et al., 2012). The detailed underlying mechanism awaits further examination.

345 Given the spatial constraints in the cytoplasm and the large volume of carboxysomes, the
346 broader distribution of carboxysomes within the cell may suggest the specific associations between
347 carboxysomes and the thylakoid membrane. Indeed, such an interaction has been deduced due to
348 the facts that RuBisCO can be found not only in the cytosol, but also near the thylakoid membranes
349 (Agarwal et al., 2009). The structural heterogeneity and dynamics of cyanobacterial thylakoid
350 membranes are fundamental to the physiological regulation of photosynthetic electron transport for
351 energy conversion (Liu, 2016). It is feasible that components in the cycle have specific subcellular
352 positioning to take advantage of the supplied energy and functionally coordinate with each other.
353 Moreover, systems analysis suggested there might be a gradient of CO_2 concentration from the cell
354 membrane to the center of the cell cytoplasm (Mangan and Brenner, 2014). Thus, changes in the
355 subcellular localization of carboxysomes, in particular along the short axis of *Synechococcus* cells,
356 probably render a means for modulating the assimilation of CO_2 within the cell.
357 Whether there are free RuBisCO proteins that are not encapsulated within carboxysomes is an
358 open question. Our confocal imaging did not demonstrate the existence of free RuBisCO in the
359 *Synechococcus* cytoplasm. It was further confirmed by our finding that no visible band of free
360 RuBisCO was determined using native-PAGE and immunoblot analysis of the soluble fraction (data
361 not shown). However, it cannot be excluded that the amount of free RuBisCO is too low to detect,
362 given the inherent resolution limitations of confocal microscopy and the sensitivity of immunoblot
363 analysis.
364 The redox state of photosynthetic electron transport chain functions as the key controller of the
365 distribution of respiratory complexes (Liu et al., 2012), photosystem composition (Fujita et al.,
366 1987), photosynthetic state transitions (Mullineaux and Allen, 1990), and the modulation of the
367 circadian clock (Ivleva et al., 2006; Wood et al., 2010). In this study, we report for the first time that
368 the redox state of photosynthetic electron transport chain located in thylakoid membranes have an
369 effect on the subcellular positioning of β-carboxysomes in *Synechococcus*. The widespread and
370 clumping distribution of carboxysomes is determined by the oxidized state of photosynthetic

electron transport chain, whereas the linear positioning of carboxysomes along the cell length is ascribed to the reduced state of photosynthetic electron transport chain (Fig. 6). Non-treated cells present similar clustering organization of carboxysomes as DCMU-treated cells, indicating that the PQ pool is oxidized upon the illumination condition, which possibly triggers the state transition to "State 1" (Mullineaux and Allen, 1990) or probably due to the high ratio of PSI and PSII in cyanobacteria (Howitt et al., 2001). Our results further reveal that the reorganization of carboxysomes appears as a long-term regulation process. It is reminiscent of the previous finding showing that the constrained diffusive dynamics of β-carboxysomes in *Synechococcus* (Savage et al., 2010).

It has been reported that *de novo* gene expression of DNA replication components in *Synechococcus* is dependent on the photosynthetic electron transport activity (Ohbayashi et al., 2013). Here we show that both DCMU and DBMIB can inhibit the synthesis of carboxysome proteins and thereby, the formation of carboxysomes (Fig. 5). Whether there are indirect effects of protein synthesis on the spatial positioning of carboxysomes needs further characterization. Our results demonstrate explicitly that DCMU and DBMIB treatments could result in distinct carboxysome positioning in the cell, whereas the carboxysome numbers, and hence probably the expression of carboxysome proteins, are comparable (Fig. 6), suggesting that the effects of electron transport inhibitors on protein synthesis seem not to correlate with the changes in carboxysome positioning.

In addition to the β-carboxysome positioning, redox regulation is also important for the β-carboxysome biosynthesis and function. Carboxysomes may preferably retain an independent redox environment from that of the cytosol, by the semi-permeable shell that can selectively exclude the entry of thioredoxin and other redox equivalents into the interior (Peña et al., 2010; Rae et al., 2013). The shell encapsulation allows the establishment of an oxidizing microenvironment within the β-carboxysome (Chen et al., 2013). The thioredoxins in the cytoplasm could reduce the redox damage to carboxysome components, and enhance the carboxysome biogenesis and maturation (Rae et al.,

2013). In addition, the independent redox modulation of the carboxysome lumen was deduced to be vital for the activities of carboxysome enzymes. The oxidizing environment could favor the activation of CcaA (Price et al., 1992) and carbonic anhydrase function of CcmM (Peña et al., 2010).

Cyanobacterial CO_2-concentrating mechanisms (CCM) comprise carboxysomes, CO_2 uptake complexes NDH-1 and HCO_3^- transports (Price et al., 2008). To date, we have demonstrated that the *in vivo* distributions of carboxysomes (this work) and NDH-1 complexes (Liu et al., 2012) were both regulated by the redox state of photosynthetic electron transport chain, suggesting the potential interplay between the two components. In addition, given that the transcriptional levels of HCO_3^- transporters were also regulated by light through photosynthetic electron flux (McGinn et al., 2004; Burnap et al., 2013), it is likely that the organization of entire CCM pathway in cyanobacteria is modulated, in an integrated network context, by the light-mediated redox regulation of photosynthetic electron flow. Therefore, thylakoid membrane remodeling during environmental adaption might play a role in the regulation of CCM pathway in the cell, which needs to be determined experimentally in future.

CONCLUSIONS

In this work, we characterized extensively the biosynthesis and spatial organization of cyanobacterial carboxysomes in response to changing light levels. Our results reveal that light intensity plays an essential role in modulating the carboxysome biosynthesis and carbon fixation capacity of cyanobacterial cells. Light-regulated carboxysome biogenesis and organization in *Synechococcus* are coordinated with photosynthetic electron flow. This study provides essential knowledge for us to modulate the β-carboxysome biosynthesis and carbon fixation in cyanobacteria. The general principles underlying the biogenesis of carboxysomes and their functional coordination with the cellular bioenergetic network could be an important consideration

when engineering functional carboxysomes and cyanobacterial CCM pathways into heterologous organisms, in specific plant chloroplasts, to boost photosynthetic performance and CO_2 assimilation activity.

MATERIALS AND METHODS

Bacterial Strains, Growth Conditions, and Generation of Constructs

Synechococcus elongatus PCC7942 was grown at 30°C with a constant white illumination in BG-11 medium (Rippka et al., 1979) in culture flasks with constant shaking, or on BG-11 plates containing 1.5% (w/v) agar. Cultures were grown in air without additional CO_2 source except for the experiment aerated with 3% CO_2. For eGFP-fusion strains, BG-11 medium was supplemented with 50 $\mu g \cdot mL^{-1}$ apramycin. Growth of cells was monitored at OD 750nm using Spectrophotometer (Jenway 6300 spectrophotometer, Jenway, UK). Three biological repeats were recorded. *Escherichia coli* (*E. coli*) strains used in this work were DH5α and BW25113. *E. coli* was grown aerobically at 30 or 37°C in Luria-Broth (LB) medium. Medium supplements were used, where appropriate, at the following final concentrations: ampicillin 100 $\mu g \cdot mL^{-1}$, chloramphenicol 10 $\mu g \cdot mL^{-1}$, apramycin 50 $\mu g \cdot mL^{-1}$ and arabinose 100 μM.

PCR products, including approximately 800 bp homologous sequence upstream and downstream of *synpcc7942_1426* (*rbcL*) or *synpcc7942_0285* (*ccmK4*), were cloned using the pGEM-T Easy cloning system (Promega). Enhanced green fluorescent protein (eGFP) fusions were created by inserting the eGFP:apramycin region amplified from the plasmid pIJ786, to the C-terminus of *rbcL* or *ccmK4*, using the Redirect strategy (Gust et al., 2002; Gust et al., 2004). Plasmids were verified by PCR and sequencing. Then the plasmids were transformed into *Synechococcus* cells following the method described earlier (Golden, 1988). Segregation of recombinant gene/protein was checked by PCR, agarose gel electrophoresis, sequencing as well as immunoblot analysis. The DNA oligonucleotides used in this work are shown in Supplemental

Table S1. Free-eGFP expressing *Synechococcus* strain was obtained using the pAM2991vector (a gift from Susan Golden, Addgene plasmid # 40248, Ivleva et al., 2005) containing eGFP.

Light and Inhibitor Treatment

Synechococcus cultures were treated with different intensities of light illuminations (10 $\mu E \cdot m^{-2} \cdot s^{-1}$ as low light, LL; 50 $\mu E \cdot m^{-2} \cdot s^{-1}$ as moderate light, ML; 100 $\mu E \cdot m^{-2} \cdot s^{-1}$ as higher light, HL). Cells were collected at the middle of exponential growth phase (to avoid self-shading) for the following imaging and biochemical analysis. The electron transport inhibitors 3-(3,4-dichlorophenyl)-1,1-dimethylurea (DCMU, Sigma, US) and 2,5-dibromo-3-methyl-6-isopropyl-p-benzoquinone (DBMIB, Sigma, US), and the protein synthesis inhibitor lincomycin were added to 20 μM, 10 μM and 400 $\mu g \cdot mL^{-1}$, respectively. Cells were adapted for 24 hours in the presence of DCMU, DBMIB or lincomycin before microscopy imaging. The free-eGFP expressing *Synechococcus* cells were induced with 1 mM isopropyl β-D-1-thiogalactopyranoside (IPTG) for 24 hours prior to confocal imaging.

Confocal Microscopy and Image Analysis

Preparation of *Synechococcus* cells for confocal microscopy was performed as described earlier (Liu et al., 2012). Laser-scanning confocal microscopy used a Zeiss LSM510 or LSM710 with a 63× or 100× oil-immersion objective and excitation at 488 nm. Live-cell images were recorded from at least five different cultures. All images were captured with all pixels below saturation. Image analysis was carried out using ImageJ software (NIH Image, Bethesda, US). Results are presented as mean ± standard deviation (SD).

Automated analysis of cell counting, the number and positioning of carboxysomes and the definition of thylakoid membranes per cell was programmed into the image analysis software Image SXM (Barrett, 2014). The carboxysomes or thylakoid membranes were identified by processing the green or red channels of confocal images using Fourier filters to highlight the carboxysomes or the

edges of thylakoid membranes. The shape and the "center of mass" of the fluorescent spots were used to determine the number and location of carboxysomes within the cell. The developed automated analysis software routines were used, in this work, for analyzing the carboxysome content and positioning.

4',6-diamidino-2-phenylindole (DAPI) staining was conducted as described previously (Smith and Williams, 2006). Briefly, cells were collected by centrifugation at 30°C and were then washed by phosphate buffer (pH 7.2) for 3 times. Cells were incubated with DAPI (20 $\mu g \cdot ml^{-1}$) in dark at 30°C for 20 min, washed by distilled water twice before loading on a BG-11 plate for confocal imaging. The DAPI-stained chromosome was visualized under the DAPI channel (excitation = 405 nm, emission = 437-552 nm).

In Vivo Carbon Fixation Assay

Cells were harvested at exponential phase under corresponding light treatments and then resuspended in RuBisCO assay buffer (100 mM EPPS, pH 8.0; 20 mM $MgCl_2$). Cell density was then calibrated by measuring OD750. Radiometric assay was carried out according to the protocol (Price and Badger, 1989) with additional cell permeabilization treatment (Schwarz et al., 1995). Cell cultures prepared in assay buffer with the same cell density were incubated with $NaH^{14}CO_3$ (final concentration at 25mM) at 30°C for 2 mins, and then permeabilized by MTA (mixed alkyltrimethylammonium bromide, Sigma, US; final concentration at 0.03%, w/v). D-ribulose 1,5-bisphosphate sodium salt hydrate (RuBP, Sigma, US) was then added with a range of concentrations (0 – 2.0 mM) to initialize the fixation. After 5 mins 10% formic acid was added to terminate the reaction. Samples were then dried on heat blocks at 95°C to remove unfixed $NaH^{14}CO_3$, and the pellets were resuspended in distilled water in the presence of scintillation cocktail (Ultima Gold XR, Perkin Elmer, US). Radioactivity measurements were carried out using scintillation counter (Tri-Carb, Perkin Elmer, US). Raw readings were processed to determine the amount of fixed ^{14}C, calibrated by blank cell samples without providing RuBP, and then converted

to the total carbon fixation rates. Carbon fixation rates of cell cultures were normalized based on the AtpB quantity from immunoblot analysis. For each experiment, at least six biological repeats were prepared. Significance was assessed using a two-tailed t-test.

Immunoblot Analysis

Synechococcus soluble fractions for sodium dodecyl sulfate-polyacrylamide gel electrophoresis (SDS-PAGE) analysis were prepared by sonication at 4°C followed by Triton treatment and centrifugation. 75 μg of proteins were loaded on 10% (v/v) denaturing SDS-PAGE gels. Gels were electroblotted onto a PVDF membrane (Bio-Rad, US). Immunoblot analyses were performed using primary mouse monoclonal anti-GFP (Life Technologies, UK), rabbit polyclonal anti-RbcL (Agrisera, Sweden), anti-ATPaseB (Agrisera, Sweden) antibodies, and horseradish peroxidase-conjugated goat anti-mouse immunoglobulin G secondary antibody (Promega, US) or anti-rabbit immunoglobulin G secondary antibody (GE Healthcare, US). Signals were visualized using a chemiluminescence kit (Bio-Rad, US). AtpB protein was used as a loading control for cell population (Zhang et al., 2012). Immunoblot protein quantification was carried out using ImageJ. For each experiment, at least three biological repeats were performed.

Transmission Electron Microscopy

Wild-type *Synechococcus* cells grown under different light conditions were pelleted and fixed for 1 hour with 4% paraformaldehyde and 2.5% glutaraldehyde in 0.05 M sodium cacodylate buffer at pH 7.2. Cells were then post-fixed with 1% osmium tetroxide for 1.5 hours, dehydrated with a series of increasing alcohol concentrations (30% to 100%), and embedded in resin. Thin sections of 70 nm were cut with a diamond knife and post-stained with 4% uranyl acetate and 3% lead citrate. Images were recorded using a FEI Tecnai G2 Spirit BioTWIN transmission electron microscope (FEI, US).

Oxygen evolution measurement

Oxygen evolution of cell cultures was measured at saturate light illumination at 30°C in a Clarke-type oxygen electrode (OxyLab 2, Hansatech). One milliliter of cell suspension with chlorophyll concentration of 20 μM was placed into the electrode chamber, aerated, and sealed from the atmosphere.

Supplemental Data

The following supplemental materials are available.

Supplemental Table S1. PCR Primers.

Supplemental Figure S1. Construction and characterization of RbcL:eGFP and CcmK4:eGFP *Synechococcus* strains.

Supplemental Figure S2. Regulation of carboxysome biosynthesis in *Synechococcus* by CO_2.

Supplemental Figure S3. Thin-section transmission electron microscopy images of wild-type *Synechococcus* cells grown under HL, ML and LL.

Supplemental Figure S4. The sizes of *Synechococcus* cells remain similar under the variation of light intensity.

Supplemental Figure S5. Light regulation of carboxysome content in RbcL:YFP cells.

Supplemental Figure S6. Relative abundance of RuBisCO in RbcL:eGFP *Synechococcus* strain under LL, ML and HL, based on confocal image analysis.

Supplemental Figure S7. ^{14}C carbon fixation rates of wild-type *Synechococcus* cells grown under LL, ML and HL, as a function of RuBP concentration (± SD, $n = 6$).

Supplemental Figure S8. Oxygen evolution analysis of *Synechococcus* cells in the presence of DBMIB and DCMU for 24 hours.

Supplemental Figure S9. Organization of carboxysomes in LL- and ML-adapted cells under the treatment of DCMU and DBMIB.

Supplemental Figure S10. The effects of DBMIB and DCMU on β-carboxysome localization in CcmK4:eGFP cells.

Supplemental Figure S11. Time-lapse confocal fluorescence imaging of RbcL:eGFP cells in the presence of DCMU and DBMIB.

ACKNOWLEDGMENTS

We thank Dr. James Hartwell for critical comments on the manuscript. We acknowledge the Liverpool Centre for Cell Imaging (CCI) for provision of confocal imaging equipment and technical assistance. We thank Prof. Ian Prior and Mrs. Alison Beckett for the support of electron microscopy.

Author contributions

Y.S. and L.-N.L. designed research; Y.S., S.C., Y.F., F.H., M.F. and L.-N.L performed research; Y.S, S.B. and L.-N.L analyzed data; Y.S. and L.-N.L. wrote the paper.

572 **Figure legends**

573 **Figure 1.** Spatial organization of β-carboxysomes in RbcL:eGFP *Synechococcus* cells. A, Confocal
574 images of a RbcL:eGFP *Synechococcus* cell. Green, eGFP labelled carboxysomes; blue, 4',6-
575 diamidino-2-phenylindole (DAPI) stained DNA; red, auto-fluorescence of the thylakoid membrane.
576 The merged channel revealed that most of the cytoplasmic volume of the *Synechococcus* cell is
577 occupied by carboxysomes and chromosomes. This subcellular organization indicated that all
578 carboxysomes in the RbcL:eGFP cell can been visualized using confocal microscopy. The confocal
579 image of the *Synechococcus* construct that expresses free eGFP illustrates that free eGFP are spread
580 throughout the cytoplasm without specific aggregation. B, Computational programming of image
581 analysis allows automatic identification of carboxysomes in cells in confocal images. Scale bar: 2
582 μm. C, Statistical determination of the spatial localization of carboxysomes within the cell revealed
583 the distribution profiles of carboxysomes along both the longitudinal and short axes of the cell (n =
584 300). The orange squares represent the relative frequency of carboxysome localization in the cell.
585 The developed automated analysis software routines were used in this work for analyzing the
586 carboxysome content and positioning.

587

588 **Figure 2.** Distinct distribution patterns of carboxysomes in *Synechococcus* under different light
589 intensities. A, Confocal microscopy images of the spatial organizations of carboxysomes in the
590 RbcL:eGFP strain grown under low light (LL, 10 $\mu E \cdot m^{-2} \cdot s^{-1}$), moderate light (ML, 50 $\mu E \cdot m^{-2} \cdot s^{-1}$)
591 and higher light (HL, 100 $\mu E \cdot m^{-2} \cdot s^{-1}$). Variations in the carboxysome content were observed under
592 different light intensities. Scale bar: 2 μm. B, Thin-section transmission electron microscopy images
593 of wild-type *Synechococcus* cells grown under LL, ML and HL (see Supplemental Fig. 3). The
594 thylakoid membranes form regular multiple parallel layers surrounding the cytoplasm. The
595 carboxysomes were observed as dark polyhedral particles (arrows) in the cytoplasm. Stronger light
596 leads to the increase in carboxysome numbers in cells. Scale bar: 1 μm. C, Computational analysis
597 of confocal images shows the average numbers of carboxysomes per cell under LL, ML and HL (n

598 = 500 for each condition). D, The positioning of carboxysomes along the normalized longitudinal
599 axis of the *Synechococcus* cell under LL, ML and HL. The relatively periodic and polar localization
600 of carboxysomes in cells were indicated (n = 500). E, The positioning of carboxysomes along the
601 normalized short axis of the *Synechococcus* cell (n = 500). HL gives rise to a wider distribution of
602 carboxysomes from the centerline of cells. F, Confocal microscopy images of CcmK4:eGFP cells
603 show the spatial positioning of carboxysomes grown under LL, ML and HL. Variations in the
604 carboxysome content were observed under different light intensities, in good agreement with those
605 of the RbcL:eGFP strain. Error bars represent standard deviation (SD, n = 500 for each condition).
606 Scale bar: 2 μm.
607
608 **Figure 3.** Characterization of the light-regulated biosynthesis process of β-carboxysomes. A, Time-
609 lapse confocal images of the LL-adapted RbcL:eGFP *Synechococcus* strain under HL treatment and
610 the HL-adapted RbcL:eGFP strain under LL treatment. Cells from the same flasks were imaged
611 under confocal microscopy once per day, for continuously 5 days. Changes in carboxysome content
612 per cell were captured. B, Analysis of the average numbers of carboxysomes based on confocal
613 images reveals an increase in carboxysome abundance induced by HL and a decline in
614 carboxysome abundance caused by LL, compared to the numbers of carboxysomes under constant
615 LL or HL treatments. Error bars represent SD (n = 250).
616
617 **Figure 4.** Light modulates the biosynthesis of β-carboxysomes and cellular carbon fixation in
618 *Synechococcus*. A, Immunoblot analysis using anti-RbcL and anti-GFP antibodies shows variations
619 of the RuBisCO content in RbcL:eGFP cells. HL triggers the accumulation of RuBisCO. Using
620 anti-RbcL antibody RbcL:eGFP strains present two bands: the upper band for RbcL-eGFP and the
621 lower band for RbcL only. AtpB was used as a loading control (Zhang et al., 2012). Gels are
622 representative of six independent experiments. B, Immunoblot analysis implies that the GFP
623 amount in RbcL:eGFP and CcmK4:eGFP cells varies under different light intensities (± SD, n = 6,

$P < 0.05$). C, Densitometry of RbcL in wild-type, RbcL:eGFP and CcmK4:eGFP cells is dependent on light intensity (± SD, $n = 6$, $P < 0.05$). D, ^{14}C carbon fixation rates of wild-type, RbcL:eGFP and CcmK4:eGFP cells under LL, ML and HL at 0.5 mM D-ribulose 1,5-bisphosphate sodium salt hydrate (RuBP, ± SD, $n = 6$). The cell density was normalized using the AtpB content (Fig. 4A). The carbon fixation rates of cells as a function of RuBP is shown in Supplemental Fig. S7. E, The carbon fixation rate per cell is proportional to the numbers of carboxysomes within the cell ($R^2 = 0.97$). The numbers of carboxysomes per cell were determined from electron microscopy images for the wild-type strain, and confocal microscopy images for RbcL:eGFP and CcmK4:eGFP strains.

Figure 5. β-carboxysome biosynthesis is regulated by photosynthetic electron flow. A, Confocal microscopy images of LL-adapted RbcL:eGFP *Synechococcus* cells after 24-hour HL treatment, in the presence of the photosynthetic electron transport inhibitors DCMU, DBMIB or the protein synthesis inhibitor lincomycin. The control images were captured in LL-adapted *Synechococcus* cells grown at LL and after 24-hour HL treatment without inhibitor treatments. Scale bar: 2 μm. B, Analysis of the average numbers of carboxysomes per cell (± SD, $n = 300$) based on the confocal images illustrates the suppression of carboxysome content with the treatments of DCMU and DBMIB, indicating that light intensity regulates the biosynthesis and assembly of carboxysomes through photosynthetic electron flux.

Figure 6. Correlation between the spatial organization of β-carboxysomes and redox state of photosynthetic electron transport chain in *Synechococcus*. A, Confocal image (left) and schematic model (right) of the HL-adapted RbcL:eGFP strain show the evenly distributed carboxysome "clusters" (orange dotted circles), each of which contains several carboxysomes assembled together in the local cytoplasmic region. B, Confocal image of HL-adapted RbcL:eGFP cells under DCMU treatment shows the clustering distribution of carboxysomes along the centerline of the cell. Scale bar: 5 μm. C, Confocal image of HL-adapted *Synechococcus* cells under DBMIB treatment shows

650 the linear distribution of carboxysomes along the centerline of the cell. Scale bar: 5 μm. D, No
651 significant changes in the cell length and width of *Synechococcus* is detected during inhibitor
652 treatments for 24 hours ($P > 0.05$, $n = 500$). Error bars represent SD. E, Average numbers of
653 carboxysomes per cell under the treatments of DCMU and DBMIB do not have remarkable changes
654 ($P > 0.05$, $n = 500$). F, Normalized spatial distribution maps of carboxysomes in cells under the
655 treatments of DCMU and DBMIB. The scale bar presents the relative frequency of carboxysome
656 localization. G, The distributions of carboxysomes along the cell length under DCMU and DBMIB
657 treatments ($n = 500$). H, DBMIB treatment results in a linear positioning of carboxysomes at the
658 centerline of HL-adapted *Synechococcus* cells, whereas the DCMU treatment leads to a wider
659 distribution of carboxysomes along the cell width ($n = 500$). Similar results were also obtained in
660 LL- and ML-adapted *Synechococcus* cells (Supplemental Fig. S9) and CcmK4:eGFP cells
661 (Supplemental Fig. 10).
662

663

Parsed Citations